Huge local elastic strains in bulk nanostructured pure zirconia materials

Taylan Ors, Fanny Gouraud, Vincent Michel, Marc Huger, Nathalie Gey, Jean-Sébastien Micha, Olivier Castelnau, René Guinebretière

Huge local elastic strains in bulk nanostructured pure zirconia materials

Taylan Ors [a,b], Fanny Gouraud [c,d], Vincent Michel [a], Marc Huger [c], Nathalie Gey [e], Jean-Sébastien Micha [f], Olivier Castelnau [a], René Guinebretière [c,*]

[a] PIMM, UMR CNRS 8006, ENSAM, CNAM, HESAM, 151 boulevard de l'Hôpital, Paris, 75013, France
[b] Université de Haute-Alsace, IS2M, UMR CNRS 7361, 3bis rue Alfred Werner, 68093 Mulhouse Cedex, France
[c] Université de Limoges, IRCER, UMR CNRS 7315, 12 rue Atlantis, Limoges, 87068, France
[d] CITRA, 16 rue Atlantis, Parc ESTER 87068 Limoges, France
[e] Université de Lorraine, Arts et Métiers Paris Tech, LEM3, UMR CNRS 7239, 57000 Metz, France
[f] CRG-IF BM32, Beamline at the European Synchrotron (ESRF) and Grenoble Alpes Université, UMR SYMMES CEA/Grenoble/ Institut of Nanosciences and Cryogenics, 17 rue des Martyrs, Cedex 9, Grenoble, 38054, France

ARTICLE INFO

Keywords:
Pure zirconia
Residual strains
X-ray laue microdiffraction
Electron backscatter diffraction

ABSTRACT

From the liquid state to room temperature, two successive solid-state phase transitions occur in pure zirconia. It is well-known that the last one (tetragonal to monoclinic) is martensitic and induces large volume variations and shear strains. Elastic and inelastic behaviors of zirconia-based materials are strongly influenced by this transition and the associated strain fields that it induces. Knowledge of strain and stress at the crystal scale is thus a crucial point. Using fully dense pure zirconia polycrystals obtained by a fuse casting process, we have determined at a sub-micrometric scale, by X-ray Laue microdiffraction, the strains map at room temperature in as-cast specimens and after a post elaboration high temperature thermal treatment. We observed that the fluctuation of deviatoric elastic strain is huge, the standard deviation of normal component being in the range of 1–2%. The heat treatment tends to even further increase this range of fluctuation, despite the development of a multiscale crack network formed during the cooling. Correspondingly, the associated stress level is also huge. It lies in the 5 GPa range with stress gradient amounting 1 GPa μm^{-1}.

1. Introduction

Dense zirconia-based materials are usually obtained through a sintering process at a temperature higher than 1000 °C or fuse cast from the liquid state. In both cases, the final materials are out of equilibrium and the presence of residual stresses plays a crucial role on the structural state of zirconia crystals and finally on the mechanical behavior of the bulk polycrystalline materials [1,2]. The coupling between solid-state phase transitions (SPT), residual stresses and mechanical response is complex. Nevertheless, for large variations of temperature, the mechanical response mainly involves two mechanisms that act at different scales: (i) the formation of a local heterogeneous stress fields, due to the intrinsic highly anisotropic elastic and thermal expansion properties of the crystals constituting the material, and (ii) the cooperative effects of intergranular interactions (so-called "microstructural effects") [3]. Engineering the mechanical characteristics at this mesoscopic scale requires a subtle relative tuning of antagonist intrinsic properties and the intergranular arrangement at the meso or nano scales. Moreover, it is well-known that physical intrinsic properties are modified when the crystal size lies in the nanometer range. Considering the mechanical properties of bulk materials, the relevant size is in the 10–100 nm range according to the Hall-Petch law [4,5]. Whatever the physical origin of internal stresses, their relaxation mechanisms are related to the elastic and inelastic behaviors of the materials under consideration. In metallic alloys, plasticity arises generally from dislocation motion. However, in oxide materials like zirconia the inelastic behavior is mainly related to microstructural effects [6] corresponding often to the formation of a multiscale crack network [7] or the formation of textured microstructures made of a very high number of crystalline domains exhibiting specific crystallographic relationships [8,9]. At high temperature, such a behavior is particularly magnified: elastic and super-elastic behaviors related to specific effects associated to phase transition processes have been observed [10,11]. It has also been experimentally demonstrated that oxide single crystals can be deformed plastically when their size lies in the 10-nm range [12].

Combining inelasticity at the microstructural scale with unconven-

* Corresponding author. IRCER, UMR CNRS 7315, 12 rue Atlantis, Limoges, 87068, France.
E-mail address: rene.guinebretiere@unilim.fr (R. Guinebretière).

tional elastic behaviors related to size effects, some intrinsically brittle oxide materials exhibit an unexpected high compliance [10,11]. Although observed at the microscale, the compliance origin often lies at the nanoscale. From this point of view, zirconia based polycrystalline materials constitute a very interesting scientific case. Indeed, pure zirconia (ZrO_2) exhibits two SPTs during cooling from the liquidus temperature. Under atmospheric pressure, in materials free of any internal or external constrains, pure zirconia solidifies into a cubic crystal structure (space group $Fm\bar{3}m$) at about 2700 °C, transforms to tetragonal (space group $P4_2/nmc$) upon cooling to 2300 °C and becomes monoclinic (space group $P2_1/c$) at 1170 °C [13]. This last SPT is a first order transition and is of martensitic type. Moreover, it induces a large volume expansion of a few percent associated to an anisotropic mechanical transformation at the crystal lattice scale that creates huge internal stresses in the material and promotes the development of a microcrack network. Nevertheless, it is well known that accurate control of this phase transition, and thus of the microcrack network formation, allows producing materials exhibiting enhanced mechanical properties [1,14]. Relaxation of thermal stresses through SPTs results in the formation of microstructures that usually involve length scales spanning at

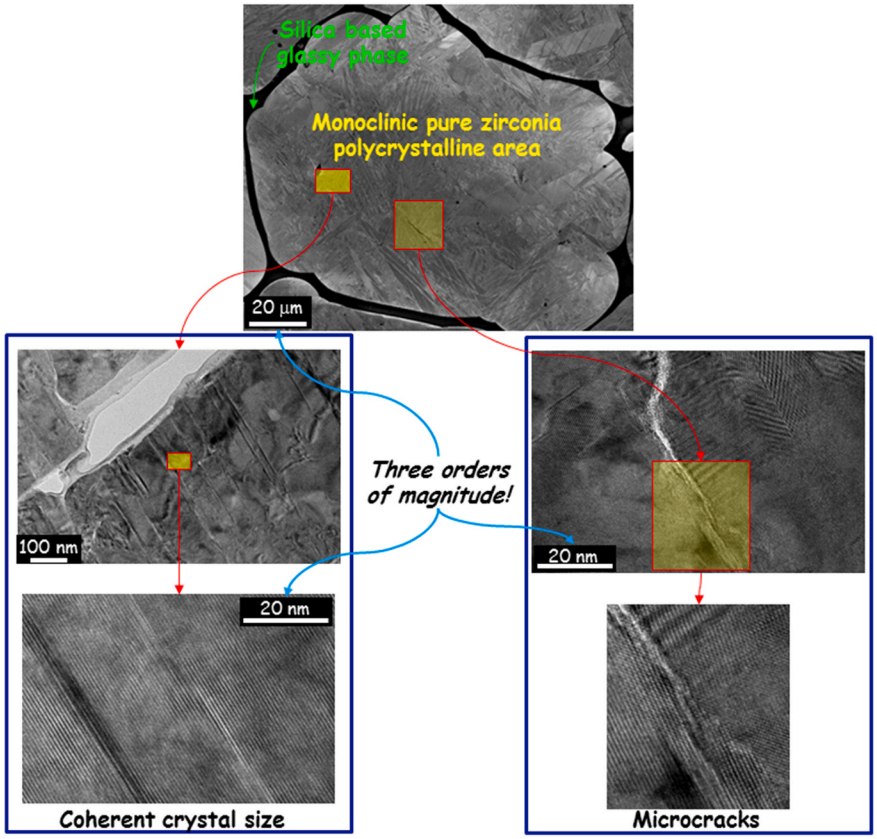

(a) Microstructure probed by electronic microscopy. The main picture was obtained by scanning electronic microscopy while the four smaller ones are transmission electron microscopy images evidencing both coherent domains and microcracks through high resolution observations.

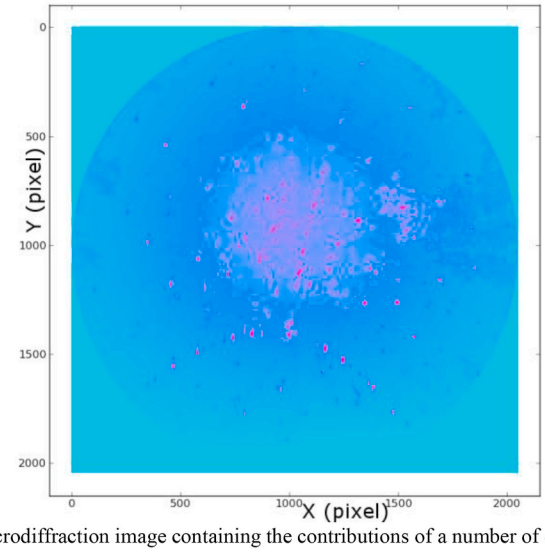

(b) one Laue microdiffraction image containing the contributions of a number of diffracting crystals

Fig. 1. Typical multiscale microstructure of a pure zirconia material elaborated through fuse-casting process and associated Laue microdiffraction pattern.

least three orders of magnitude from the crystal size to the grain size. As an illustrative example, we show in Fig. 1a the multi-scale microstructure of pure zirconia manufactured through fuse-casting process. Coherent domains have a typical size of few tens of nanometers and they are part of larger polycrystalline volumes of usually a few tens of micrometers.

Since the publication of the founding article of Garvie et al. [1], strain and stress induced SPTs in zirconia have been studied using theoretical modelling approach [15] and the microstructure induced by these transitions has been predicted through phase field modelling during the last decade [18–20]. Concerning experimental approaches [8,16,17], it is worth noting that they have been essentially focused on *doped* zirconia. The introduction of aliovalent cations in substitution to zirconium induces in most cases a significant reduction of the difference between the *a, b* and *c* cell parameters of zirconia. As the level of the residual stresses is partially related to the mismatches between the different cell parameters of the non-cubic zirconia phases [21], higher strain and stress levels are expected to be generated within *pure* zirconia polycrystalline samples compared to doped ones. This often leads to the breakage of these materials associated to a partial relaxation of the internal stresses. Consequently, the true level of strain induced by the phase transitions is in fact not well-known. Accordingly, as far as we know, direct experimental measurement of the actual level of local internal residual strain distribution at room temperature in pure zirconia crystals within bulk polycrystalline samples has up to now never be performed.

The purpose of this paper is to determine the level of local strains in such pure zirconia polycrystals. Recent studies on fused cast zirconia have introduced very interesting samples made of sub-millimetric pure zirconia areas embedded into a glassy phase [22,23]. Such microstructure is the result of a phase separation process occurring in the liquid state in the pseudo binary phase SiO_2–ZrO_2 phase diagram [24,25]. It has already been demonstrated [9] that each of these areas come from the same cubic single crystal at high temperature. It means that all these monoclinic submicrometric crystals of one given area are in fact belonging to crystallographic variants of the same cubic grain generated by the successive SPTs occurring during the cooling of the sample. We show in this article by X-ray Laue microdiffraction that the successive SPTs associated with volume variation and anisotropic thermal expansion of monoclinic zirconia [26,27] induce local strains of a few percent into the pure zirconia crystals. Associated internal stresses are in the GPa range. We demonstrate experimentally that the global residual stresses at the scale of the sub-millimeter former cubic volume are at least ten times smaller than local values. This feature avoids the general breakage of the monoclinic polycrystalline areas and offers a unique scientific case, allowing direct illustration of the coupling between SPTs and anisotropy of thermal expansion of pure zirconia on one side and the generation of stresses in the GPa range on the other side.

2. Material and methods

The fabrication process of the samples has already been described in details in Ref. [23] and thus is recalled only briefly here. In all the cases, they have been manufactured by the Saint-Gobain company. The raw materials are melted and then poured into a mold. A careful cooling process allows avoiding the global breakage of the zirconia blocks that are sub-metric in size. As shown in Fig. 1a, the sub-millimetric areas of ZrO_2 embedded into silica-based glass are fully dense and are made of a very large number of constituting crystals. The specimens investigated come from large blocks (size ~250 × 400 × 450 mm^3) containing 94 wt % of pure zirconia. The remaining 6 wt% is a glassy phase seen in dark grey in Fig. 1a. One block was cut in order to obtain one slice close to its surface and another slice in the central part of the block. Two equivalent samples were extracted from each slice and one of them was heat treated at 1500 °C for 1 h in order to observe the effects of the m→t and the reverse t→m transitions on the internal strain state. Samples nomenclature is given in Table 1. Each sample was cut to a final size of 5 × 5 × 10 mm^3 and these pieces were then mounted in resin, grounded and polished mechanically with the procedure described in Ref. [23].

Laue microdiffraction experiments were carried out at the French CRG beamline BM32 at the European synchrotron radiation facility (ESRF), Grenoble, France [28]. A MARCCD165 detector (79.14 μm pixel size, 2048 × 2048 pixels, 16 bits dynamic) was used to record the diffraction patterns. The sample-detector distance was ~70 mm. As for the precise geometrical calibration of the setup (position and orientation of the detector with respect to the incoming X-ray beam, and sample position) which is important for an accurate analysis of Laue microdiffraction patterns, we used a stress-free germanium single crystal that was systematically measured before the investigation of each sample. The precise sample positioning was achieved thanks to an optical microscope with a narrow depth of field (~2 μm). The set-up geometry and calibration procedure are detailed in Ref. [28].

A polychromatic beam with an energy ranging between 5 and 22 keV was used. This beam was focused down to a cross section of ~300 × 300 nm^2 (at the focal point) by Kirkpatrick-Baez mirrors installed on the beamline. The sample stage was inclined by 40° with respect to the direction of the X-ray primary beam. The surface of the sample was scanned with the X-ray beam along two orthogonal axes to create a mesh of scan points. According to the X-ray energy range, the attenuation length in zirconia lies between 5 and 40 μm and thus, accounting for the setup geometry, one can estimate that the X-rays probe a surface layer of 10 μm thickness. With this setup, a single crystal of monoclinic zirconia creates a Laue pattern containing several tens of diffraction spots. As evidenced in Fig. 1a, our sample is made of a very large number of coherently diffracting nanosized crystals misoriented with each other. Thus, even with an X-ray beam of sub-micrometer cross section, taking into account the penetration depth lying in the ten microns range, at each position of the sample with respect to this beam, the probed volume contains few thousand of monoclinic crystals, a number of which are diffracting simultaneously. Thus, each Laue microdiffraction image contains a number of Laue microdiffraction patterns (see Fig. 1b). The experimental Laue microdiffraction patterns that we recorded are therefore particularly difficult to handle with standard analysis routines (peak search & indexing) developed for large crystals well separated in orientation space. Here, we followed the method introduced by Ref. [29] and based on the use of Electron Backscatter Diffraction (EBSD) data as initial average guesses (~0.5 deg accuracy) for the lattice orientation of the diffracting crystals. This allows us to index unambiguously superimposed Laue patterns of several nanosized crystals for a reliable determination of their corresponding local strain states. All the experimental work reported in this paper has been processed following this EBSD-assisted Laue microdiffraction method [29].

Hence, the micro-texture of the sample was first determined by EBSD with a Zeiss SUPRA 40 SEM equipped with Bruker QUANTAX system. An accelerating voltage of 15 kV and a working distance of ~15 mm were used throughout the analysis. EBSD measurements were carried out with the same setup. For each sample, regions of interest (ROI) were defined and measured. Step size for the EBSD scan was 0.2 μm. Standard QUANTAX software was used for the data treatment. The position of ROIs were then identified by tiny marks machined by focused ion beam in the SEM so that it can be easily located later on with the optical microscope mounted on the Laue setup.

The Laue patterns images were treated by the software “LaueTools” (https://gitlab.esrf.fr/micha/lauetools) which is presented in detail in

Table 1
Sample nomenclature with respect to sampling position and heat treatment.

Sample label	Position in the block	State
1	Surface	As-cast
2a	Center	As-cast
2b	Center	Heat treated

Ref. [30]. Additional self-developed python codes were also used to treat and combine data obtained from EBSD and Laue microdiffraction [29, 31].

The details of deviatoric strain measurement by the Laue microdiffraction method are discussed in Refs. [29,30,32] after the original paper [33]. Elastic deformations of the crystal lattice can be assessed by the refinement of the diffraction peaks angular shifts with respect to reference unstrained crystal counterparts. The reciprocal lattice vectors $\overrightarrow{q_{hkl}}$ of the deformed lattice can be expressed by the following equation:

$$\overrightarrow{q_{hkl}} = \mathbf{U}.\mathbf{B}.\overrightarrow{G_{hkl}}$$

where $\overrightarrow{G_{hkl}}$ is the reciprocal lattice vector of the undeformed lattice for a given *hkl* reflection, **U** is the rotation matrix to transform the coordinate system from orthogonalized crystal basis to laboratory basis [34] and **B** describes the mechanical transformation of the lattice associated to the elastic strain of interest here. Tensor **U.B** is proportional to the inverse of the transpose of the mechanical deformation gradient (usually denoted **F**), from which the symmetric elastic strain can be derived. For a diffraction pattern containing contributions from many crystals, the knowledge of a good initial guess for **U** obtained from the EBSD data is necessary to refine the Laue peak positions and estimate subsequently the strain for each identified crystal with **B** [29]. Here, the considered unstrained lattice parameters of monoclinic zirconia are taken from Howard et al. [35]: $a = 0.51505$ nm, $b = 0.52116$ nm, $c = 0.53173$ nm, and $\beta = 99.230°$.

During the data treatment, the crystal orientations with the most dominant contribution in the diffraction pattern were analyzed. The exact orientation of each crystal is refined for each pattern and finally the strain refinement is done accounting, on average, for more than 60 Laue spots of different *hkl* indexes per image. During the experiment at BM32, the wavelength of Laue spots was not measured as this requires an additional time-consuming scanning of the incident beam energy [36]. Therefore, only the deviatoric part of the strain tensor can be extracted from the data, not the volumetric part as the volume of the crystal cell cannot be determined. In the following, only results concerning the deviatoric elastic strain are presented and discussed.

3. Results

3.1. Distribution of elastic strain

A relevant example of microstructure for sample 1 (SEM image obtained by backscattered electrons) is shown in Fig. 2a. As already illustrated in Fig. 1, the pure zirconia areas which constitutes the ROI are made of a huge number of monoclinic zirconia crystals and are embedded in a glassy phase (in black in Fig. 2a). The local texture of this ROI was determined by EBSD measurements. Superimposition of the

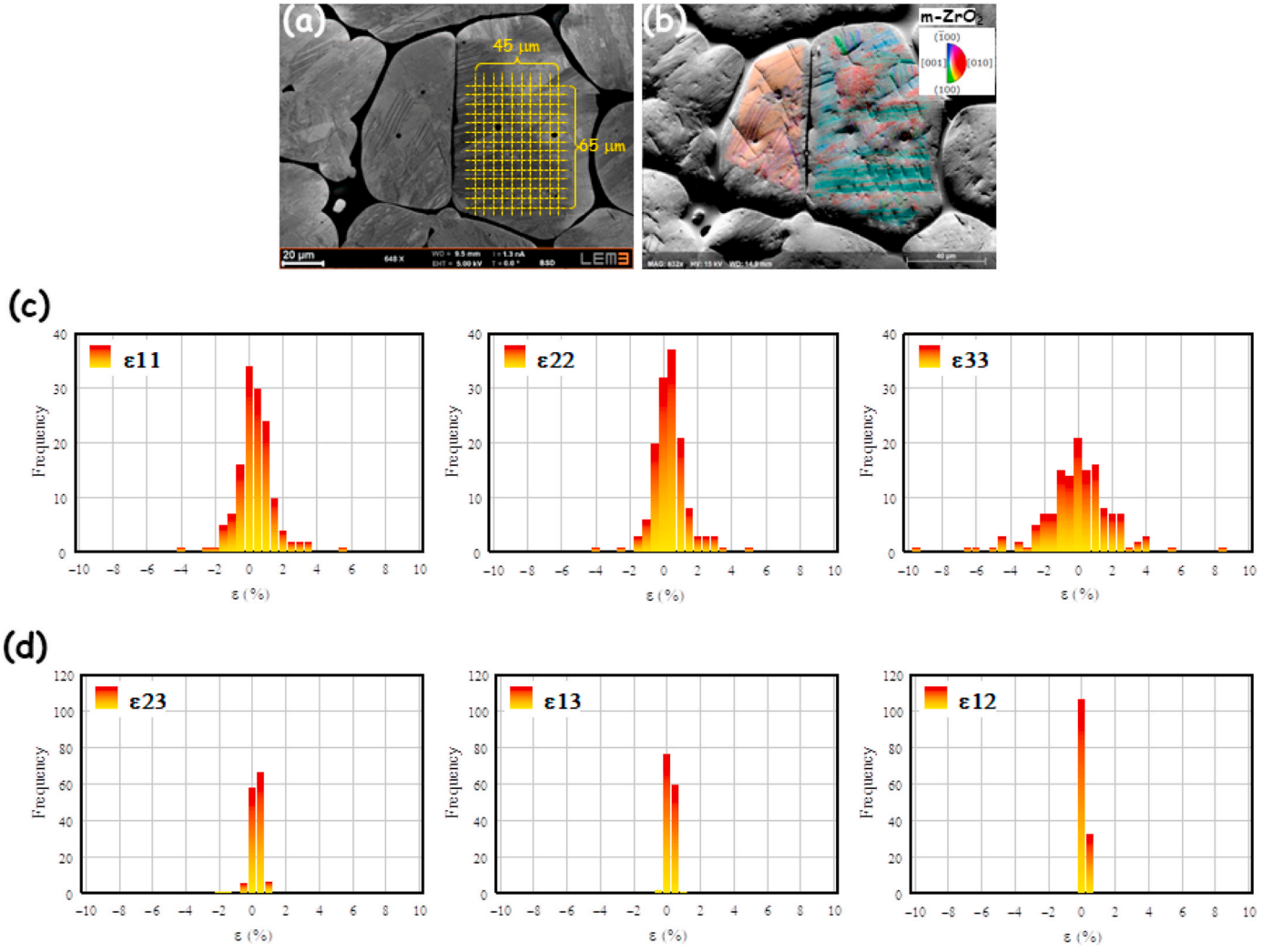

Fig. 2. Sample 1. (a) SEM image of the studied ROI; (b) local texture determined by EBSD measurement; Distribution of (c) normal and (d) shear strain components expressed in the crystal reference frame.

inverse pole figures map upon the SEM image is reported in Fig. 2b. The orientation of the monoclinic crystals is inherited from the martensitic t→m SPT [37] and the resulting microstructure exhibits a banded feature that has been observed experimentally many times. P.M. Kelly and L.R. Francis Rose published a review on this aspect [38]. Such a microstructure related to the martensitic transition has also been predicted by phase field modelling [18].

As the whole ROI corresponds to a unique parent cubic crystal appearing at the transition between the liquid and the solid states, the orientations of all the diffracting crystals result from the two successive SPTs during cooling and thus correspond to the 24 possible variants [9]. Nevertheless, the diffracting crystals corresponding to the same variant are slightly misoriented with each other and this induces a slight splitting of Laue diffraction spots [29]. Laue microdiffraction patterns were recorded in the whole ROI reported in Fig. 2a, comprising an area of 45 × 65 μm^2 and scanned with a step size of 5 μm along two orthogonal directions, thus making 140 elementary volumes. With the method indicated above, all the Laue patterns were fully indexed.

The corresponding distributions of all components of the deviatoric elastic strain are shown in Fig. 2c and d. The strain tensors are expressed in a reference frame ($\vec{e_1}$, $\vec{e_2}$, $\vec{e_3}$) attached to the crystal lattice. The $\vec{e_1}$ and $\vec{e_2}$ vectors are colinear to the [100] and [010] directions respectively while $\vec{e_3}$ is perpendicular to the (001) planes (therefore $\vec{e_3}$ lies at ~9 deg from [001] due to the unright angle β). These distributions show a wide range of strain values (see also Table 2), especially for the normal component ε_{33} associated to variation of lattice spacing for (001) planes for which the standard deviation, indicating the fluctuation of ε_{33} within the ROI, is larger than 2%. The ε_{33} strain distribution is roughly symmetric, and the mean value is close to typically a tenth of the standard deviation, *i.e.* ~0.27% (see Table 2). Similar behavior is observed for the two others normal components ε_{11} and ε_{22} that exhibit mean values and standard deviations typically half of those observed for ε_{33} . All the three shear components (Fig. 2d) show a much narrower distribution with maximum measured values of ~1% and standard deviations and mean values roughly one order of magnitude smaller than those observed for ε_{33}.

The strain distributions given Fig. 2c and d have been obtained from data coming from the whole probed area of size of 45 × 65 μm^2. As already discussed, it includes different crystallographic variants generated by the SPTs. In order to extract the strain state of a set of crystals belonging mainly to a unique variant, we probed a smaller ROI of 10 μm by 10 μm with a step size of 1 μm. The mesh used is drawn on top of the EBSD map of the considered ROI reported in Fig. 3a and the spatial distribution of normal strain ε_{33} is superimposed upon the probed ROI in Fig. 3b. Finally, the distributions of the three normal strain components ε_{11}, ε_{22} and ε_{33} are drawn in Fig. 3c. The mean values and the standard deviations are reported in Table 2.

The highest strain value measured in this ROI is smaller than that one determined in the larger area including several variants (see Fig. 2) and the standard deviation is typically half of that one observed for a larger ROI. Looking at the insert drawn in Fig. 3b, it is interesting to see that sometimes red colored squares (high strain) are adjacent to white (low strain) or even green ones (high strain with opposite sign). This result shows the presence of very strong strain fluctuations between one elementary probed volume to the next adjacent volume. The corresponding strain gradient is huge, of the order of 10^{-2} μm^{-1}.

Because of the very large size (sub-metric) of the fuse-cast blocks, a high thermal gradient is observed during the cooling process [23] even if the complete cooling lasts for several days. In order to check the potential influence of this gradient onto the local strain, we determined the strain distribution in sample 2a located near the central part of the initial block. The Laue microdiffraction scan was performed over a ROI of 40 × 40 μm^2 with a step of 4 μm. This ROI was again selected from the EBSD map as belonging to one parent cubic crystal (see Fig. 4a). The strain distribution with respect to the crystallographic axes is drawn in Fig. 4b. A comparison between the ε_{33} strain component measured respectively in samples 1 and 2a is given Fig. 4c, mean values and standard deviations are also reported in Table 2. The histograms are not directly fully comparable because the extension of the scanned areas is not exactly the same, nevertheless they both contain more than one variant. The main difference is the presence of longer tail and twice larger standard deviation for sample 1.

Due to the intrinsic physical properties of zirconia, zirconia-based materials are very often used at high temperature. High temperature post treatments, done after the elaboration process on pure zirconia crystals, induce the m→t reverse transition. During heating, each monoclinic zirconia crystal is transformed into a tetragonal one, but during the following cooling stage each of these tetragonal crystals usually transforms into a large number of monoclinic crystals with respect to a twinning process. Successive heat treatments of zirconia at temperature higher than the m→t SPT result in a refinement of the microstructure (see for example [18]). The m⇔t transitions are associated with significant mechanical deformations including shear and volume variation of the crystal lattice and the intergranular stresses are partially relaxed through the formation of the microcrack network. One interesting question is the coupling between the microstructural refinement and the variation of the local internal strain within zirconia crystals. In order to get some experimental information about this process, we have measured the local deviatoric strain distribution present in sample 2b that has been heat treated at 1500 °C (see Table 1).

A typical SEM image obtained for sample 2b is reported in Fig. 5a. We superimposed to this image the inverse pole figure giving the main orientations of the monoclinic variants in an area of 20 × 20 μm^2. One of the interesting aspects is that the main yellow/green colored region is circumscribed by two parallel cracks located at, or very close to the variant boundaries on each long side of this area. The presence of these two cracks probably originates from the relaxation of stresses linked to the volume variation associated to the t→m SPT. It is of course well known that the formation of microcracks is an efficient stresses relaxation process in zirconia-based materials. We realized Laue microdiffraction measurements in a small ROI containing one of these cracks. A 5 × 5 μm^2 area was scanned with a step of 0.5 μm. The corresponding mesh is drawn in Fig. 5c and the ε_{33} strain values are reported on Fig. 5d as a color scale 2D map. The strain variation along this direction is very large with a standard deviation of 2.605% (see Table 2). This confirms the huge strain values into an area made of a large number of coherently diffracting domains exhibiting similar global crystallographic orientations and thus belonging to the same variant. Another interesting observation is the low values of the deviatoric strain close to the microcrack (see the part of the strain map inside the superimposed blue ellipse). Around the microcracks, at distance of few hundreds of

Table 2
Mean values and standard deviations of the measured deviatoric strains, expressed in %.

Sample label		Mean value						Standard deviation					
		ε_{11}	ε_{22}	ε_{33}	ε_{12}	ε_{13}	ε_{23}	ε_{11}	ε_{22}	ε_{33}	ε_{12}	ε_{13}	ε_{23}
1	Large ROI (Fig. 2)	0.139	0.136	−0.275	−0.005	−0.025	−0.050	1.119	1.085	2.193	0.349	0.179	0.135
	Small ROI (Fig. 3)	−0.160	−0.150	0.310	0.080	0.018	0.028	0.671	0.629	1.287	0.146	0.108	0.099
2a	As received (Fig. 4)	−0.010	−0.156	0.166	−0.027	0.007	0.014	0.660	0.664	1.311	0.129	0.110	0.057
2b	Heat treated (Fig. 5)	−0.159	−0.189	0.349	0.023	0.032	0.015	1.315	1.300	2.605	0.205	0.222	0.093

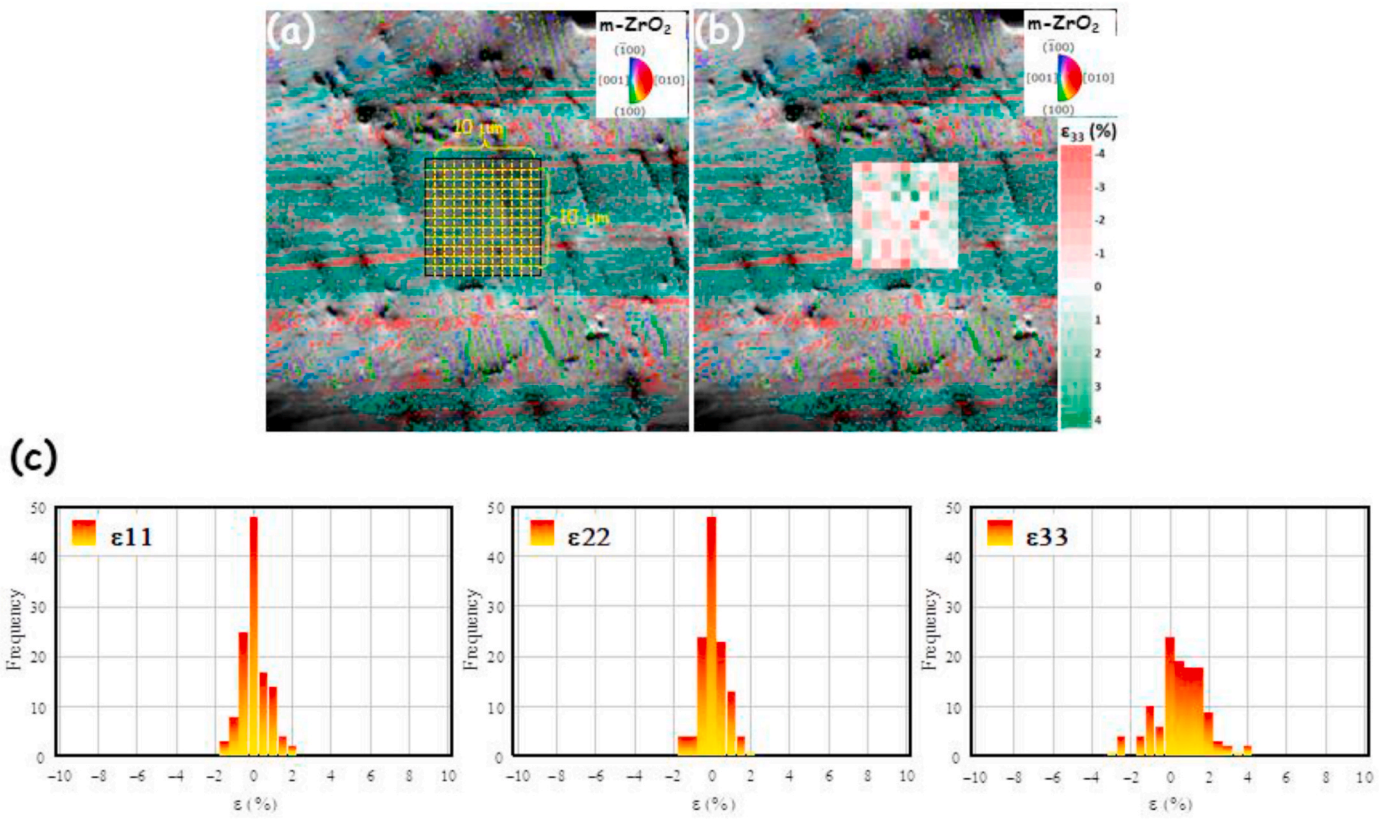

Fig. 3. Strain level and distribution in a volume corresponding mainly to one monoclinic variant for sample 1. (a) Inverse Pole Figure map superimposed upon the SEM image, and grid scanned by Laue microdiffraction. (b) Map of ε_{33} obtained by Laue. (c) Distribution of normal strain components.

nanometers, the strain level is below 1%, *i.e.* significantly smaller than its value a few micrometers further away from the crack! The corresponding histogram of the normal strain ε_{33} is reported in Fig. 5b and for a comparison, we have also plotted in this Figure the distribution of the same strain component for a similar area on sample 2a. According to Fig. 5b, it appears that heat-treatment promoting the m→t and the reverse t→m SPTs induces an increase of the span of strain distribution. As reported in Table 2, the standard deviation is roughly twice larger after thermal treatment. Moreover, the mean value is also significantly higher.

3.2. Associated residual stresses

As already discussed, diffraction techniques provide information about the mean lattice *d*-spacing in the gauge volume containing diffracting crystals. In the case of Laue microdiffraction, only the positions of Laue spots on the X-ray detector are analyzed as a measure of the direction of the diffraction vector of each *hkl* spot. As the energy of Laue spots could not be measured in the present experiment, Laue images are insensitive to any isotropic dilation of the crystal lattice transforming the crystal in a homothetic way. Therefore, only the deviatoric part of the elastic strain tensor can be evaluated. Basically, those five independent strain components already provide a very rich information about the local mechanical state of the material, as seen above. Nevertheless, it is more customary to consider the associated stress level.

The *complete* stress tensor in a crystal cannot be evaluated from the sole knowledge of the deviatoric strain. As for the *deviatoric* stress tensor, it can be evaluated from the sole knowledge of the deviatoric strain only under specific conditions: the elastic stiffness of the crystal should be such that a hydrostatic stress only produces an isotropic strain. In other word, the anisotropic Hooke's law should not couple the spherical (or volumetric) and deviatoric parts of the stress and strain tensors. These conditions are met only for crystals with a cubic lattice or with an isotropic elastic behavior, as explained in the supplementary material of [39]. Such conditions are clearly not met for monoclinic zirconia single crystals, since for example C_{33} (two indexes Voigt notation) is about ~1.6 times smaller than C_{22} and only one order of magnitude larger than C_{15}, C_{25}, C_{35}, and C_{46} [40]. It can be shown for example that the corresponding Young modulus in a single crystal ranges between ~100 GPa and 330 GPa depending on the direction of loading with respect to the crystal lattice, with by far no cubic symmetry.

Therefore, to provide a rough estimation of the deviatoric stress associated with the measured strain reported before, we have computed the isotropic stiffness tensor that is closest to the single crystal elastic stiffness of the monoclinic phase. We have used for that the method proposed by Morin et al. [41] involving a minimization of the log-Euclidian distance between both tensors. This leads to a Young modulus $E = 242$ GPa and a Poisson ratio $\nu = 0.29$. Using these values, one obtains that the strain fluctuations of about ±2% found for specimen 1 are associated with a fluctuation of the deviatoric stress that lies in the 5 GPa range. The strain gradient of $\sim 10^{-2}$ µm^{-1} measured in section 3.1 provides a gradient of deviatoric stress in the range of 1 GPa µm^{-1}. These estimations are without accounting for the local hydrostatic pressure and its fluctuation within the polycrystalline zirconia aggregate, which might further increase them. In summary, huge fluctuations of local stress level accompanied by huge stress gradients are found in the as-cast and heat-treated specimens!

4. Discussion

The present work is largely based on the unique capabilities of the Laue microdiffraction technique to estimate the field of elastic strain in deformed materials. The lateral spatial resolution of the technique is directly related to the beam size (~300 nm in our case) whereas the

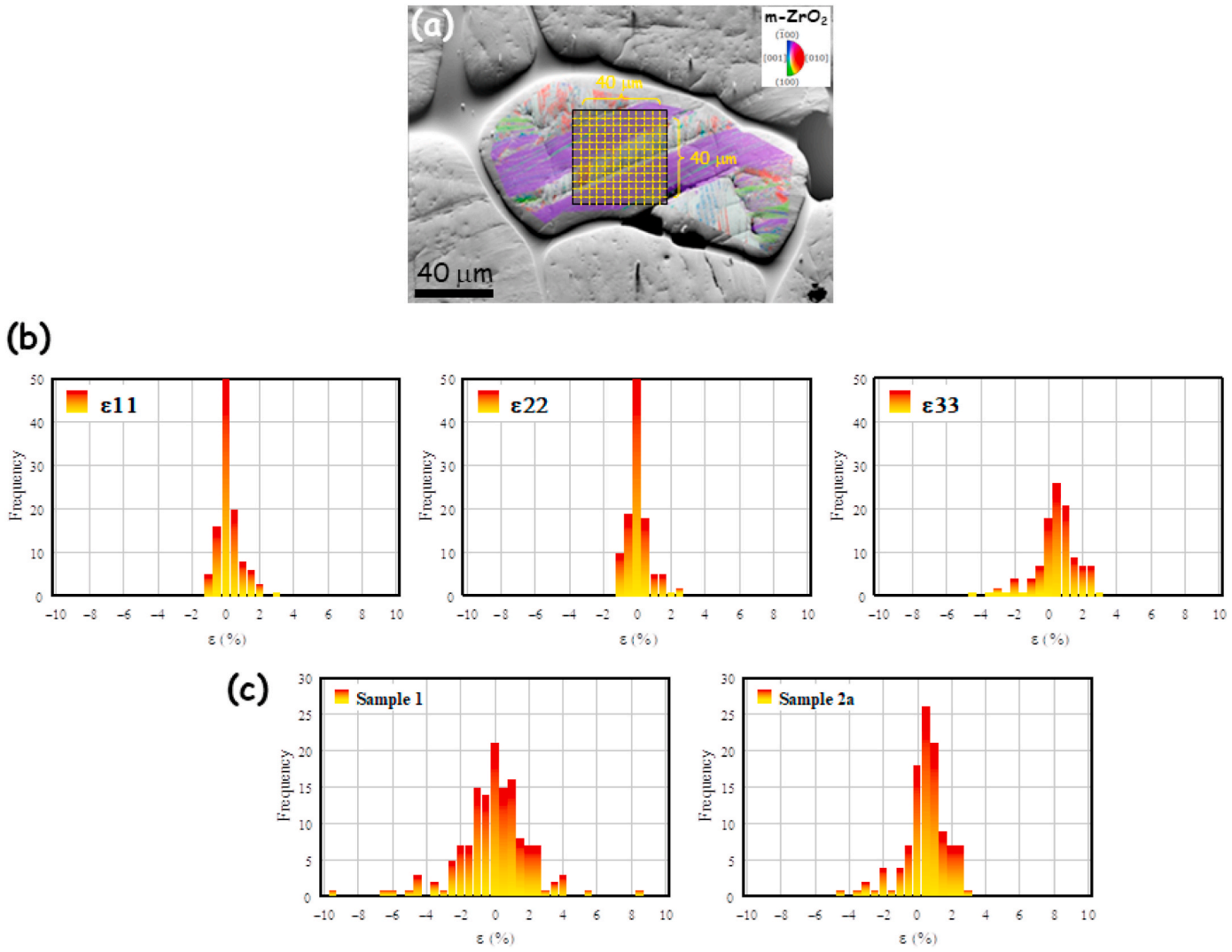

Fig. 4. Influence of the location of the sample into the zirconia block. (a) Microstructure of sample 2a. (b) Corresponding distribution of normal strain obtained by the Laue microdiffraction scanning of the area shown in (a). (c) Comparison of normal strain ε_{33} for specimens 1 and 2a.

spatial resolution along the beam direction is dictated by the x-ray attenuation length in the material, ~10 µm for ZrO_2 and the used X-ray beam energy range. The associated gauge volume contains a very large number of crystals from the same variant. It should be mentioned that most of the published work using this Laue technique has been carried out on materials with a cubic structure. There are only few published applications of Laue microdiffraction to stress field measurements in materials with lower crystal symmetries, *e.g.* Refs. [42–44]. The advantage of lower lattice symmetry is a larger number of Laue spots on the X-ray detector, which improves significantly the accuracy of stress determination as shown by Ref. [45], but at the same time the detector can become crowded by too many overlapping Laue spots, rendering the indexation of Laue patterns more complex as discussed above. On their work on natural quartz, Chen et al. [42] indicate that they reach a strain resolution of $\sim 10^{-4}$. Besides some partial results shown in Ref. [29], there is to the best of our knowledge only one published paper in which Laue microdiffraction has been used to investigate zirconia [46], but the study was focussed on sintered yttria stabilized zirconia (for dental applications) for which the internal stress level is expected to be lower than in our fuse-cast pure material, as explained above. The authors found a standard deviation of the stress of ~500 MPa in their microstructure. They could make use of only 6 to 12 Laue spots in each image to index the Laue patterns. Such a small number reduces the strain accuracy and thus tends to broaden the associated strain distribution. In the present study, use was made of more than 60 Laue spots on each image to estimate the elastic strain, leading to a strain accuracy of about 10^{-4} [29].

The accuracy of elastic strain measured by Laue microdiffraction has also been evaluated in a few recent papers by combining Monte Carlo and experimental studies [45,47–49]. In all these studies, the authors conclude that accuracy is in the order of 10^{-4}. It can be further improved by using an image correlation technique to detect the slight distortion of Laue pattern due to the elastic strain, as in Ref. [50], but as the strain fluctuations in zirconia are found to be two orders of magnitude larger than the accuracy, using this Laue-DIC was not found necessary here. Interestingly, Poshadel et al. [48] found that the uncertainty on the shear components of the strain tensor is about twice as large as that on normal components. Here, we found that the standard deviation of the shear strain distribution, which is around 10^{-3} on average (Table 2), is much larger than the expected resolution of the setup but much smaller than the fluctuations of normal strains. We are therefore highly confident on the obtained strain and stress values are accurate.

Each area that we have characterized corresponds to only one parent cubic crystals appearing at the liquid to solid states transition. In all the studied cases, the strain distributions are roughly symmetric. According to the associated stress estimation, except for the heat-treated specimen, one can conclude that the average strain and stress levels of the global

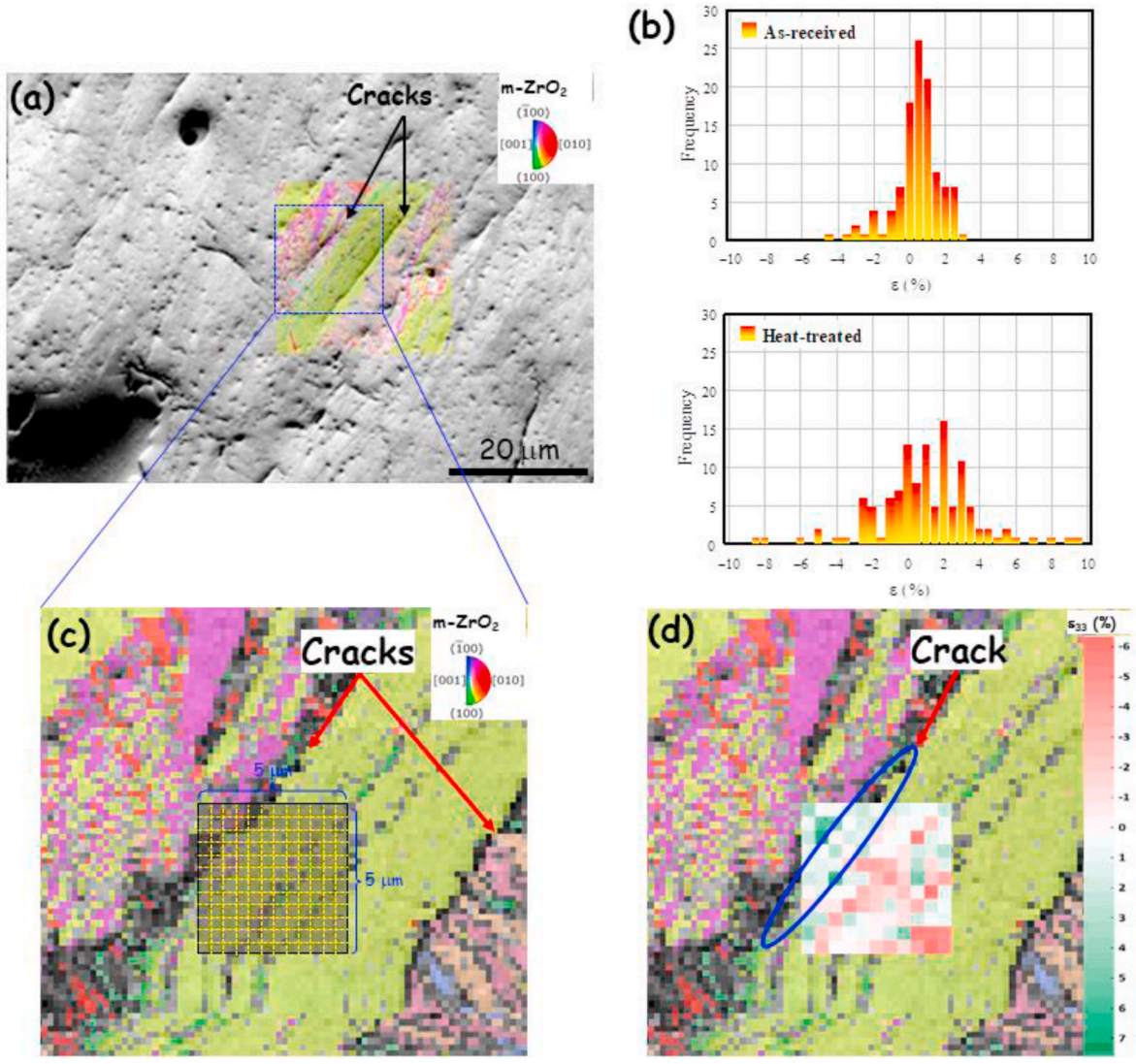

Fig. 5. Influence of a post-elaboration heat treatment at 1500 °C (Sample 2b). (a) SEM microstructure and Inverse Pole figure map obtained by EBSD. (b) Distribution of ε_{33} obtained by Laue microdiffraction, compared to sample 2a. (c) Mesh showing the area scanned by Laue microdiffraction. (d) Map of ε_{33} superimposed upon the EBSD map.

area corresponding to the parent cubic crystal are at least one order of magnitude smaller than the local one. The larger part of internal strain probably appears through the t→m transition during the cooling process. At the corresponding temperature, the viscosity of the glassy phase embedding the zirconia polycrystalline areas is very low [23] and the glass can thus easily accommodate the global deformation associated to each former parent cubic crystal.

We compared the strain state of two samples located respectively at the surface and near the center of the initial sub-metric block. We observed that higher deviatoric strain is observed in the sample located near the surface of the block. Nevertheless, the global feature of the strain distributions is very similar. The cooling process of the whole zirconia block takes several days [23] and the cooling of the surface part is faster than it is in the center of the block. Nevertheless, the global observed strain state with elastic deformations of the crystals of up to few percent is not related to the temperature gradient within the block but to both the thermal expansion anisotropy and the successive SPTs and in particular to the t→m transition that is associated with a large mechanical transformation including huge volume variations. The kinetic of the structural phase transition is certainly different at the surface and in the bulk of the large block but the induced local volume variations are similar and consequently the associated elastic strains are lying in the same range.

At the scale of few micrometers to few tens of micrometers we observed the well-known banded microstructure [37] evidencing the presence of areas that are made each by a large number of coherently diffracting domains. As evidenced by EBSD, each band corresponds to a given crystallographic variant and we often observed the presence of microcracks between different variants as illustrated in Fig. 5. We were able to demonstrate by local Laue microdiffraction with a sub-micrometer step scan that the deviatoric elastic strain in crystals located very near the microcrack is typically ten time smaller than the one recorded in crystals located few micrometers away from the crack. This perfectly illustrates the role and the efficiency of the microcrack network for the stress relaxation at this mesoscale. The strain state is related to internal stresses created by the SPTs and the thermal expansion anisotropy. It developed thus at the crystal scale, *i.e.* at a sub-micron scale. Formation of microcracks induces a relaxation process. Nevertheless, it is worth noting that only a few microns away from the relaxed crystals, high level of strain are again measured.

Thermal post-treatment at temperature higher than the m→t transition induces, during the cooling stage, the formation of numerous different monoclinic crystals from each tetragonal crystal. As a result, the mean size of the monoclinic crystals after the post-treatment is lower

than before and thus the number of interfaces between such crystals is higher. A comparison of the measured strain values between the treated and untreated samples clearly demonstrate that the thermal treatment does not lead to a decrease of the strain level but, on the contrary, it makes it increase. It also seems to increase the span of strain distribution. According to the prediction of M. Mamivand et al. [18] obtained by phase field modelling, we think that this increase of the strain level is due to the thermal expansion anisotropy of monoclinic crystals that promotes the appearance of dilatational strains. In fact, because of this anisotropy, an increase of the number of incoherent or semi-coherent interfaces increases the global strain level. In order to accommodate the cell parameters mismatch, the atomic planes are stretched or compressed causing an important strain field, that is probably associated to the formation of distribution of lattice *d*-spacing into the monoclinic crystals. Such a *d*-spacing distribution must induce the presence of diffuse scattering close to the diffraction peaks. We will discuss this last aspect in a forthcoming paper based on X-ray scattering experiments realized *in situ* at high temperature.

The local strains that we evidenced at the crystal size (tens of nm) are of a few percent and, as written above this correspond to deviatoric stresses lying in the GPa range. Total stress level, *i.e.* accounting also for the hydrostatic part, could not be evaluated here but one can anticipate that it lies in the same range if not at an even higher value. It is interesting to note that very high pressure may promote the formation of orthorhombic zirconia that is observed in the pure zirconia state diagram at pressure higher than 2 GPa [40,51]. Although, many works have been done on the zirconia SPTs, the knowledge of the true structural path between the t and m phases is indeed still an open question. Orthorhombic phases belonging to different space groups (*Pbcm*, *Pbc*2_1, *Pnam*) can be intermediate between the t and m phases or alternative to the formation of the m phase [13,40,52,53]. Thus, the knowledge of the local stress level is a prerequisite in order to explore the structural behavior of zirconia associated to the breaking of the four-fold symmetry axis that is characteristic of the t-zirconia.

5. Conclusions

Using a combination of EBSD and Laue X-ray microdiffraction measurements, the distribution of local deviatoric elastic strain present in polycrystalline materials free of external constrain and made of pure monoclinic zirconia crystals has been determined. The two successive solid-state phase transitions occurring during the material cooling stage and the strong anisotropy of the thermal expansion of monoclinic zirconia induce huge strain fluctuation of a few percent and up to roughly 10%. An evaluation of the associated residual stress shows that it lies in the GPa range with gradients as high as 1 GPa μm^{-1}. The dense polycrystalline areas that have been studied here are made of thousands of monoclinic crystals coming from the two successive SPTs and belonging to all the 24 crystallographic possible variants. The average global strain within these areas is typically one order of magnitude smaller than the local one. Stress relaxation mainly occurs by the development of a microcrack network. At the crystal scale, the level of strain remains at the value of few percent even after post-processing thermal treatment; this is mainly related to the local crystallographic mismatch at the incoherent or semi-coherent interfaces between coherently diffracting domains. This effect is certainly enhanced by the high anisotropy of the thermal expansion of monoclinic zirconia.

CRediT authorship contribution statement

Taylan Ors: prepared and realized all the Laue microdiffraction experiments, performed all the electron microscopy experiments, interpreted the Laue microdiffraction data with the help of Jean Sébastien Micha. **Fanny Gouraud:** defined the convenient samples that were prepared by Fanny Gouraud and Taylan Ors. **Vincent Michel:** prepared and realized all the Laue microdiffraction experiments. **Marc Huger:** proposed the scientific topic, defined the convenient samples that were prepared by Fanny Gouraud and Taylan Ors. . **Nathalie Gey:** performed all the electron microscopy experiments. **Jean-Sébastien Micha:** prepared and realized all the Laue microdiffraction experiments. **Olivier Castelnau:** proposed the scientific topic, prepared and realized all the Laue microdiffraction experiments, interpreted the Laue microdiffraction data with the help of Jean Sébastien Micha. **René Guinebretière:** proposed the scientific topic, prepared and realized all the Laue microdiffraction experiments, defined the convenient samples that were prepared by Fanny Gouraud and Taylan Ors, interpreted the Laue microdiffraction data with the help of Jean Sébastien Micha, wrote the manuscript with strong contributions by Taylan Ors and Olivier Castelnau and participation of all the authors.

Declaration of competing interest

The authors declare that they have no known competing financial interests or personal relationships that could have appeared to influence the work reported in this paper.

Acknowledgements

This work was done in the frame of the ASZTECH research program funded by the ANR (ANR-12-RMNP-0007). We acknowledge the ESRF and the French Collaborating Research Group (F-CRG) for provision of synchrotron radiation facilities beamtimes and beamline staff for their assistance. The authors are thankful to I. Cabodi and O. Bories (Saint-Gobain CREE) for the supply of the bulk zirconia-based materials.

References

[1] R.C. Garvie, R.H. Hannink, R.T. Pascoe, Ceramic steel? Nature 258 (1975) 703–704.
[2] L.L. Lange, Transformation toughening, J. Mater. Sci. 17 (1982) 225–263.
[3] J.W. Christian, The Theory of Transformations in Metals and Alloys, Pergamon, Oxford, 1981.
[4] E.O. Hall, The deformation and ageing of mild steel: III Discussion of Results, Proc. Phys. Soc. Lond. 64 (1951) 747–753.
[5] N.J. Petch, The cleavage strength of polycrystals, J. Iron Steel Inst. London. 173 (1953) 25–28.
[6] P.E. Reyes-Morel, J.S. Cherng, I.W. Chen, Transformation plasticity of CeO_2-stabilized tetragonal zirconia polycrystals: II, pseudoelasticity and shape memory effect, J. Am. Ceram. Soc. 71 (1988) 648–657.
[7] I. Pozdnyakova, G. Bruno, A.M. Efremov, B. Clausen, D. Hughes, Stress-dependent elastic properties of porous microcracked ceramics, Adv. Eng. Mater. 11 (2009) 1023–1029.
[8] X.M. Zeng, A. Lai, C.L. Gan, C.A. Schuh, Crystal orientation dependence of the stress-induced martensitic transformation in zirconia-based shape memory ceramics, Acta Mater. 116 (2016) 124–135.
[9] M. Humbert, N. Gey, C. Patapy, E. Joussein, M. Huger, R. Guinebretière, T. Chotard, A. Hazotte, Identification and orientation determination of parent cubic domains from EBSD maps of monoclinic pure zirconia, Scripta Mater. 63 (2010) 411–414.
[10] A. Lai, Z. Du, C.L. Gan, C.A. Schuh, Shape memory and superelastic ceramics at small scales, Science 341 (2013) 1505–1508.
[11] Z. Du, X.M. Zeng, Q. Liu, C.A. Schuh, C.L. Gan, Superelasticity in micro-scale memory ceramic particles, Acta Mater. 123 (2017) 255–263.
[12] I. Issa, J. Amodeo, J. Rethore, L. Joly-Pottuz, C. Esnouf, J. Morthomas, M. Perez, J. Chevalier, K. Masenelli-Varlot, *In situ* investigation of MgO nanocube deformation at room temperature, Acta Mater. 86 (2015) 295–304.
[13] M. Smirnov, A. Mirgorodsky, R. Guinebretière, Phenomenological theory of lattice dynamics and polymorphism of ZrO_2, Phys. Rev. B 68 (2003) 104106.
[14] E.H. Kisi, Zirconia engineering ceramics - old challenges, new ideas, Key Eng. Mater. (1998) 153–154. Trans. Tech. Pub., Switzerland.
[15] A.P. Mirgorodsky, M.B. Smirnov, P.E. Quintard, T. Merle-Mejean, Strain induced destabilization of crystals: lattice dynamics of the cubic-tetragonal phase transition in ZrO_2, Phys. Rev. 52 (1995) 9111–9114.
[16] P.M. Kelly, C.J. Ball, Crystallography of stress-induced martensitic transformations in partially stabilized zirconia, J. Am. Ceram. Soc. 69 (1986) 259–264.
[17] A.A. Sobol, Y.K. Voronko, Stress-induced cubic-tetragonal transformation in partially stabilized ZrO_2: Raman spectroscopy study, J. Phys. Chem. Solid. 65 (2004) 1103–1112.
[18] M. Mamivand, M.A. Zaeem, H. El Kadiri, L.Q. Chen, Phase field modeling of the tetragonal-to-monoclinic phase transformation in zirconia, Acta Mater. 61 (2013) 5223–5235.

[19] M. Mamivand, M.A. Zaeem, H. El Kadiri, Phase field modeling of stress-induced tetragonal-to-monoclinic transformation in zirconia and its effect on transformation toughening, Acta Mater. 64 (2014) 208–219.
[20] E. Moshkelgosha, M. Mamivand, Phase field modeling of crack propagation in shape memory ceramics - application to zirconia, Comput. Mater. Sci. 174 (2020) 109509.
[21] A.H. Heuer, M. Ruhle, D.B. Marshall, On the thermoelastic martensitic transformation in tetragonal zirconia, J. Am. Ceram. Soc. 73 (1990) 1084–1093.
[22] C. Patapy, N. Gey, A. Hazotte, M. Humbert, D. Chateigner, R. Guinebretiere, M. Huger, T. Chotard, Mechanical behavior characterization of high zirconia fused-cast refractories at high temperature: influence of the cooling stage on microstructural changes, J. Eur. Ceram. Soc. 32 (2012) 3929–3939.
[23] C. Patapy, M. Huger, T. Chotard, R. Guinebretiere, N. Gey, A. Hazotte, M. Humbert, Solidification structure in pure zirconia liquid molten phase, J. Eur. Ceram. Soc. 33 (2013) 259–268.
[24] H. Kin, P.C. McIntyre, Spinodal decomposition in amorphous metal–silicate thin films: phase diagram analysis and interface effects on kinetics, J. Appl. Phys. 92 (2002) 5094–5102.
[25] A. Gaudon, A. Dauger, A. Lecomte, B. Soulestin, R. Guinebretiere, Phase separation in sol–gel derived ZrO_2–SiO_2 nanostructured materials, J. Eur. Ceram. Soc. 25 (2005) 283–286.
[26] F. Frey, H. Boysen, T. Vogt, Neutron powder investigation of the monoclinic to tetragonal phase transformation in undoped zirconia, Acta Crystallogr. B. 46 (1990) 724–730.
[27] R. Guinebretière, S. Arnaud, N. Blanc, N. Boudet, E. Thune, D. Babonneau, O. Castelnau, Full reciprocal space mapping up to 2000 K under controlled atmosphere: the multi-purpose QMAX furnace", J. Appl. Crystallogr. 53 (2020) 650–661.
[28] O. Ulrich, X. Biquard, P. Bleuet, O. Geaymond, P. Gergaud, J.S. Micha, O. Robach, F. Rieutord, A new white beam X-ray microdiffraction setup on the BM32 beamline at the European Synchrotron Radiation Facility, Rev. Sci. Instrum. 82 (2011) 15–21.
[29] T. Örs, J.S. Micha, N. Gey, V. Michel, O. Castelnau, R. Guinebretiere, EBSD-assisted Laue microdiffraction for microstrain analysis, J. Appl. Crystallogr. 51 (2018) 55–67.
[30] O. Robach, J.S. Micha, O. Ulrich, B. Devincre, T. Hoc, G. Daveau, V. Consonni, J. Petit, Analyse avancée des contraintes et des gradients d'orientation par microdiffraction Laue des rayons X, in: R. Guinebretière, P. Goudeau (Eds.), Rayons X et Matière, vol. 5, ISTE Editions Ltd., London, 2017, pp. 83–142.
[31] A.M. Boullier, O. Robach, B. Ildefonse, F. Barou, D. Mainprice, T. Ohtani, K. Fujimoto, High stresses stored in fault zones: example of the Nojima fault (Japan), Solid Earth 9 (2018) 505–529.
[32] J. Hektor, J.B. Marijon, M. Ristinmaa, S.A. Hall, H. Hallberg, S. Iyengar, J.S. Micha, O. Robach, F. Grennerat, O. Castelnau, Evidence of 3D strain gradients associated with tin whisker growth, Scripta Mater. 144 (2018) 1–4.
[33] J.S. Chung, G. Ice, Automated indexing for texture and strain measurement with broad-bandpass X-ray microbeams, J. Appl. Phys. 86 (1999) 5249–5255.
[34] W.R. Busing, H.A. Levy, Angle calculations for 3- and 4-circle X-ray and neutron diffractometers, Acta Crystallogr. 22 (1967) 457–464.
[35] C.J. Howard, R.J. Hill, B.E. Reichert, Structure of the ZrO_2 polymorphs at room temperature by high-resolution neutron powder diffraction, Acta Crystallogr. B44 (1988) 116–120.
[36] O. Robach, J.S. Micha, O. Ulrich, O. Geaymond, O. Sicardy, J. Härtwig, F. Rieutord, A tunable multicolour 'rainbow' filter for improved stress and dislocation density
[37] K.J. Bowman, I.W. Chen, Transformation texture in zirconia, J. Am. Ceram. Soc. 76 (1993) 113–122.
[38] P.M. Kelly, L.R. Francis Rose, The martensitic transformation in ceramics – its role in transformation toughening, Prog. Mater. Sci. 47 (2002) 463–557.
[39] J. Petit, O. Castelnau, M. Bornert, F. Zhang, F. Hofmann, A.M. Korsunsky, D. Faurie, C. Le Bourlot, J.S. Micha, O. Robach, O. Ulrich, Laue-DIC: a new method for improved stress field measurements at the micron scale, J. Synchrotron Radiat. 22 (2015) 980–994.
[40] G. Fadda, L. Truskinovsky, G. Zazotto, Unified Laudau description of the tetragonal, orthorhombic, and monoclinic phases of zirconia, Phys. Rev. B 66 (2002) 174107.
[41] L. Morin, P. Gilormini, K. Derrien, Generalized Euclidian distances for elasticity tensors, J. Elasticity 138 (2020) 221–232.
[42] K. Chen, M. Kunz, E. Zepeda-Alarcon, M. Sintubin, H.R. Wenk, Compressional residual stress in Bastogne boudins revealed by synchrotron X-ray microdiffraction, Geophys. Res. Lett. 43 (2016) 6178–6185.
[43] A. Bhowmik, I.P. Dolbnya, T.B. Britton, N.G. Jones, G. Sernicola, C. Walter, P. Gille, D. Dye, W.J. Clegg, F. Giuliani, Finn, Using coupled micropillar compression and micro-Laue diffraction to investigate deformation mechanisms in a complex metallic alloy $Al_{13}Co_4$, Appl. Phys. Lett. 108 (2016) 111902.
[44] K.S. Befus, M. Manga, C. Stan, N. Tamura, Volcanoes erupt stressed quartz crystals, Geophys. Res. Lett. 46 (2019) 8791–8800.
[45] F.G. Zhang, M. Bornert, J. Petit, O. Castelnau, Accuracy of stress measurement by Laue microdiffraction (Laue-DIC method): the influence of image noise, calibration errors and spot number, J. Synchrotron Radiat. 24 (2017) 802–817.
[46] H.A. Bale, N. Tamura, P. Coelho, J.C. Hanan, Interface residual stresses in dental zirconia using Laue micro diffraction, in: Proc. 8th International Conference on Residual Stress, 2008.
[47] F. Hofmann, S. Eve, J. Belnoue, J.S. Micha, A.M. Korsunsky, Analysis of strain error sources in micro-beam Laue diffraction, Nucl. Instrum. Methods Phys. Res. Sect. A Accel. Spectrom. Detect. Assoc. Equip. 660 (2011) 130–137.
[48] A. Poshadel, P. Dawson, G. Johnson, Assessment of deviatoric lattice strain uncertainty for polychromatic X-ray microdiffraction experiments, J. Synchrotron Radiat. 19 (2012) 237–244.
[49] E. Plancher, J. Petit, C. Maurice, V. Favier, L. Saintoyant, D. Loisnard, N. Rupin, J.-B. Marijon, O. Ulrich, M. Bornert, J.-S. Micha, O. Robach, O. Castelnau, On the accuracy of elastic strain field measurements by Laue microdiffraction and high-resolution EBSD: a cross-validation experiment, Exp. Mech. 56 (2016) 48349.
[50] J. Petit, O. Castelnau, M. Bornert, F. Zhang, F. Hofmann, A.M. Korsunsky, D. Faurie, C. Le Bourlot, J.S. Micha, O. Robach, O. Ulrich, Laue-DIC: a new method for improved stress field measurements at the micron scale, J. Synchrotron Radiat. 22 (2015) 980–994.
[51] O. Ohtaka, T. Yamanaka, S. Kume, E. Ito, A. Navrotsky, Stability of monoclinic and orthorhombic zirconia: studies by high-pressure phase equilibria and calorimetry, J. Am. Ceram. Soc. 74 (1991) 505–509.
[52] S.H. Guan, X.J. Zhang, Z.P. Liu, Energy landscape of zirconia phase transitions, J. Am. Chem. Soc. 137 (2015) 8010–8013.
[53] S. Liu, W. Hu, Y. Zhnag, J. Xiang, F. Wen, B. Xu, J. He, D. Yu, Y. Tian, Z. Liu, Metastable adaptive orthorhombic martensite in zirconia nanoparticles, J. Appl. Crystallogr. 47 (2014) 684–691.